Eur. Phys. J. C 30, 359–365 (2003)
Digital Object Identifier (DOI) 10.1140/epjc/s2003-01294-1

THE EUROPEAN PHYSICAL JOURNAL C

Geometric scaling in exclusive processes

S. Munier[1,a], S. Wallon[2,b]

[1] Institute for Theoretical Physics, University of Heidelberg, Philosophenweg 19, 69120 Heidelberg, Germany
[2] Laboratoire de Physique Théorique, Université Paris XI, centre d'Orsay, bâtiment 211, 91405 Orsay cedex, France

Received: 27 May 2003 / Revised version: 7 July 2003 /
Published online: 29 August 2003 –

Abstract. We show that according to the present understanding of the energy evolution of the observables measured in deep-inelastic scattering, the photon–proton scattering amplitude has to exhibit geometric scaling at each impact parameter. We suggest a way to test this experimentally at HERA. A qualitative analysis based on published data is presented and discussed.

1 Introduction

The striking phenomenon of geometric scaling discovered in the HERA data [1] has triggered a wide interest. The inclusive deep-inelastic scattering (DIS) cross section $\sigma(x,Q)$ measured as a function of the photon virtuality Q and the Bjorken variable x, was shown to depend on the single combined variable $Q^2 \cdot (x/x_0)^{\lambda_0}$ where $\lambda_0 \sim 0.3$ and $x_0 \sim 3 \cdot 10^{-4}$. Empirically, this scaling turns out to be valid for $x \leq 10^{-2}$ and for all available values of Q^2 (in practice, for $Q^2 = 0$ to $400\,\mathrm{GeV}^2$). Geometric scaling has also been found more recently in deep-inelastic scattering off nuclei [2].

A similar scaling behavior was discussed a long time ago in the framework of elastic proton–proton scattering [3,4]. At that time, an impact parameter analysis revealed that the rise of the cross section as a power of the center-of-mass energy was due to an effective growth of the size of the interaction region, which was almost black in its center. Geometric scaling in γ^*–p scattering was discovered in the context of the discussion of saturation effects, and is often considered as evidence for the fact that the proton looks already quite black, or "saturated", at HERA.

The scaling variable turns out to be the dimensionless ratio of the photon virtuality Q and the so-called saturation scale, which has the following dependence upon the Bjorken variable:

$$Q_\mathrm{s}(x) \sim 1\,\mathrm{GeV} \cdot \left(\frac{x}{x_0}\right)^{-\lambda_0/2} . \qquad (1)$$

The latter is believed to characterize the mean transverse momentum of partons with longitudinal momentum fraction x. The growth of this typical momentum scale with energy $W = Q/\sqrt{x}$ is understood within several different formulations of dense parton evolution [5–12] which technically lead to non-linear integro-differential equations. Geometric scaling was seen in numerical simulations of these models [13,14]. It was shown to be consistent with QCD evolution in the range in which it is verified in the data [15]. In [16–18], it was derived from perturbative QCD for Q above the saturation scale as a feature of the Balitsky–Fadin–Kuraev–Lipatov (BFKL) equation [19,20] with appropriate boundary conditions. In [21], the symmetry of the quantity $Q/Q_\mathrm{s} \cdot \sigma(Q/Q_\mathrm{s})$ under the interchange of Q and Q_s already noticed in [1] was interpreted as possible evidence for a proton looking like a collection of independent dipoles of typical size $1/Q_\mathrm{s}$. The generalized vector dominance model combined with the color dipole model as formulated in [22] also leads to geometric scaling. More recently, geometric scaling for all Q^2 was deduced from the critical behavior of the correlation function of Wilson lines which appears at small x in a near-light-cone Hamiltonian formalism [23]. This approach looks fundamentally different from the other ones, in the sense that it does not rely on the parton model.

Most of the latter discussions were only concerned with inclusive quantities. The proton was assumed to be an homogeneous disk, and its size large with respect to the size of the probe, so that boundary effects could be neglected. The reason for these assumptions is the technical complication of the saturation equations when the full dependence upon transverse coordinates is taken into account.

However, one knows that the saturation scale itself depends on the impact parameter. Indeed, it is related to the density of partons inside the proton, which obviously decreases smoothly when one moves from the center to the periphery. The saturation scale in the ideal case described before was only a kind of effective one. Actually, it is theoretically not clear what this scale is in a real proton, because all momenta from Λ_QCD to Q are a priori expected to contribute to the cross sections.

[a] e-mail: munier@tphys.uni-heidelberg.de
[b] e-mail: Samuel.Wallon@th.u-psud.fr

The importance of impact parameter studies for the phenomenology of saturation effects at HERA was explained in [24]. A theoretical discussion of the impact parameter dependence of the saturation scale $Q_{\rm s}(x,b)$ was provided in [25]. In the latter paper, some arguments were put forward in favor of a "local" geometric scaling, which would manifest itself in the fact that cross sections for exclusive processes only depend on the ratio of scales $Q/Q_{\rm s}(x,b)$. Let us also stress that geometric scaling for exclusive processes has recently been predicted qualitatively in the context of the discussion of generalized parton distributions [26].

The aim of this paper is to show that "local" geometric scaling is testable experimentally. In the first section, we explain why this new scaling is expected. We then propose a method to investigate it at HERA. Finally, we discuss the qualitative results obtained so far by applying our method to the data.

2 Saturation and geometric scaling

In this section, we show how local scaling appears within different theoretical approaches. We consider the idealized process of scattering of a dipole of size $1/Q$ off a dipole of size $1/\Lambda$. Λ and Q are fixed momentum scales, which are taken in the perturbative region in the following discussion, and the ordering $Q > \Lambda$ is assumed. The small dipole is called "projectile" and the large one "target". In the end, Λ will be formally extrapolated to $\Lambda_{\rm QCD}$. We denote by $y \equiv \log(1/x)$ the maximum rapidity available at CM energy $W = Q/\sqrt{x}$.

2.1 Global and local scaling above the saturation scale from linear evolution

We explore here the perturbative picture of high energy scattering. We consider dipole–dipole scattering at fixed impact parameter b as given by the BFKL equation. We assume that b is larger than the sizes of the initial-state dipoles: $b \gg 1/Q, 1/\Lambda$. The Mellin representation of the solution of the BFKL equation then reads [27, 28]

$$\mathcal{A}_{\rm d}(y,Q,b) = \frac{1}{2}\frac{1}{Q^2\Lambda^2 b^4}\int\frac{{\rm d}\gamma}{2{\rm i}\pi}(1-2\gamma)d(\gamma)\left(16b^2Q\Lambda\right)^{2\gamma}{\rm e}^{\bar{\alpha}_{\rm s}y\chi(\gamma)}\,, \tag{2}$$

where the integration goes over a line in the complex plane parallel to the imaginary axis and intersecting the real axis between 0 and 1. In our conventions, the S and T matrices are related by $S = 1 - T$, so that generally speaking the amplitudes are essentially real at high energy. This is true in particular for the BFKL solution (2). The following standard notations have been used: $\bar{\alpha}_{\rm s} = \alpha_{\rm s}N_c/\pi$ and $\chi(\gamma) = 2\psi(1) - \psi(\gamma) - \psi(1-\gamma)$. The function $d(\gamma) = \alpha_{\rm s}^2/(16\gamma^2(1-\gamma)^2)$ is the Mellin transform of the elementary dipole–dipole elastic amplitude with respect to the ratio of their sizes, with appropriate normalization.

The forward amplitude $\mathcal{T}_{\rm d}$ is obtained by integrating (2) over the impact parameter b. As formula (2) holds only in the large b approximation, we must set the lower bound of the integral to a number of the order of the size of the largest interacting dipole. We choose $1/(4\Lambda)$ and check the consistency a posteriori. The forward amplitude then reads

$$\mathcal{T}_{\rm d}(y,Q) = 2\pi\int_{1/(4\Lambda)}^{\infty}{\rm d}b\,b\,\mathcal{A}_{\rm d}(y,Q,b) = \frac{8\pi}{Q^2}\int\frac{{\rm d}\gamma}{2{\rm i}\pi}d(\gamma)\left(\frac{Q}{\Lambda}\right)^{2\gamma}{\rm e}^{\bar{\alpha}_{\rm s}y\chi(\gamma)}\,. \tag{3}$$

One checks the normalizations by computing the total cross section, using the optical theorem which reads $\sigma = 2\mathcal{T}_{\rm d}$ in our conventions. Setting $y = 0$, one recovers the well-known expression of the elementary (lowest order) dipole–dipole cross section [29].

Let us recall how one obtains geometric scaling from this equation. One is interested in the large y region, where a saddle point gives the dominant contribution to the integral in (3). Expanding the function $\chi(\gamma)$ to second order around $\gamma = 1/2$, the amplitude (3) reads

$$\mathcal{T}_{\rm d}(y,Q) = \frac{4\pi\alpha_{\rm s}^2}{\sqrt{\pi a^2 y}}\frac{1}{\Lambda^2} \times\exp\left\{\omega y - \frac{1}{2}\log(Q^2/\Lambda^2) - \frac{1}{4a^2y}\log^2(Q^2/\Lambda^2)\right\}\,, \tag{4}$$

with the definitions $\omega \equiv 4\bar{\alpha}_{\rm s}\log 2$ (the BFKL intercept) and $a^2 \equiv 14\zeta(3)\bar{\alpha}_{\rm s}$. At fixed y, the amplitude becomes large (of the order of the area of the target) when the argument of the exponential is positive, which occurs below the scale $Q = Q_{\rm s}(y)$ satisfying the relation

$$Q_{\rm s}^2(y) = \Lambda^2{\rm e}^{\lambda y},\ \text{with}\ \lambda \equiv a^2\left(\sqrt{1+4\omega/a^2}-1\right)\,. \tag{5}$$

Note that this formula can be compared with the form of the saturation scale previously quoted (1) provided one makes the identifications $\lambda \to \lambda_0$ and $\Lambda \to 1\,{\rm GeV}\cdot x_0^{\lambda_0/2}$. The equation $Q^2 = Q_{\rm s}^2(y)$ defines the so-called critical line below which, per definition, the amplitude (3) is large and non-linear corrections prove to be necessary to ensure probability conservation. The interesting feature of (4) is that it can be rewritten as a function of the ratio of the variables Q and $Q_{\rm s}$, up to some approximation. Putting (4) and (5) together, one arrives at

$$\mathcal{T}_{\rm d}(y,Q) = \frac{4\pi\alpha_{\rm s}^2}{\sqrt{\pi a^2 y}}\frac{1}{\Lambda^2} \times\exp\left\{-\frac{1}{a^2y}\log^2\frac{Q}{Q_{\rm s}(y)}\right\}\left(\frac{Q}{Q_{\rm s}(y)}\right)^{-\sqrt{1+4\omega/a^2}}\,. \tag{6}$$

The factor which still contains the rapidity alone is slowly varying, hence it can be approximated by its value for a fixed typical rapidity y_0. Moreover, if Q is sufficiently

close to Q_s, one can trade the exponential for 1. This approximation applies when $|\log Q/Q_\mathrm{s}| \ll a^2 y\sqrt{1+4\omega/a^2}$. Introducing the notation $\gamma \equiv (\sqrt{1+4\omega/a^2})/2$, the amplitude can be rewritten

$$\mathcal{T}_\mathrm{d}(Q, Q_\mathrm{s}(y)) = \frac{4\pi\alpha_\mathrm{s}^2}{\sqrt{\pi a^2 y_0}} \frac{1}{\Lambda^2} \left(\frac{Q_\mathrm{s}^2(y)}{Q^2}\right)^\gamma , \qquad (7)$$

which exhibits geometric scaling.

To make contact with HERA phenomenology, one has to set $\Lambda = \Lambda_\mathrm{QCD}$ and to average the projectile size r with a weight given by the squared photon wave function. This is the well-known dipole model [30, 31] which provides an appealing and useful picture of DIS in the leading-logarithmic approximation of QCD. The virtual photon–proton cross section reads

$$\sigma_{\gamma^* p}(y, Q) = \int \mathrm{d}^2 r\, \psi^\dagger_{\gamma^*}(r, Q) \otimes \psi_{\gamma^*}(r, Q) \cdot 2\mathcal{T}_\mathrm{d}(y, 1/r) \ . \qquad (8)$$

ψ_{γ^*} is the photon wave function on a $q\bar{q}$ color dipole. Besides the transverse size r and virtuality of the photon Q, this wave function also depends on the longitudinal momentum fraction z of the antiquark. The notation "$\otimes$" stands for an integration over z. For negligible quark masses, $\psi^\dagger_{\gamma^*}(r, Q) \otimes \psi_{\gamma^*}(r, Q)$ is a function of rQ only which vanishes rapidly at large rQ [1]. Thus the scaling property of the dipole–proton amplitude (7) is transmitted to the photon–proton cross section itself which then exhibits the same behavior as the amplitude $\mathcal{T}_\mathrm{d}$ in (7).

The formula just established would give a reasonable description of the data in a limited kinematical range, provided one considers ω and a^2 as effective parameters. Indeed, the values given by the leading order BFKL equation are known to be incompatible with the data on one hand, and to receive large corrections from next-to-leading order terms on the other hand. The parameters have to be adjusted such that $\lambda \sim \lambda_0 \sim 0.3$ and $\gamma \sim 1$ [21,32]. Then the formulae (1) and (5) show that the choice $x_0 = 3 \cdot 10^{-4}$ implies $\Lambda_\mathrm{QCD} = 300\,\mathrm{MeV}$, which is reasonable. To obtain more reliable expressions, neglected effects such as diffusion into the infrared have to be taken into account. As shown in [17], the latter have sizable effects both on the parametric form of the saturation scale (5) and on the expression of the amplitude (7), but do not spoil the overall picture.

The previous analysis can be taken over to the impact parameter dependent amplitude (2) in a straightforward way. The steepest-descent method gives (see [33])

$$\mathcal{A}_\mathrm{d}(y, Q, b) = \frac{128\pi\alpha_\mathrm{s}^2}{(\pi a^2 y)^{3/2}} \log(16 b^2 Q\Lambda) \qquad (9)$$

$$\times \exp\left\{\omega y - \log(16 b^2 Q\Lambda) - \frac{1}{a^2 y}\log^2(16 b^2 Q\Lambda)\right\} \ .$$

This amplitude is again of order 1 for $Q = Q_\mathrm{s}$, the saturation scale Q_s being given by

$$Q_\mathrm{s}^2(y, b) = \frac{1}{256\Lambda^2 b^4} \exp(\lambda y) \ . \qquad (10)$$

Within the approximations already made in the inclusive case, the amplitude can then be expressed as a function of Q and Q_s only:

$$\mathcal{A}_\mathrm{d}(Q, Q_\mathrm{s}(y, b)) = \frac{64\alpha_\mathrm{s}^2}{\sqrt{\pi a^2 y_0}}(2\gamma - 1) \cdot \left(\frac{Q_\mathrm{s}^2(y, b)}{Q^2}\right)^\gamma , \qquad (11)$$

where the saturation scale now depends on the impact parameter b. Thus we see that the amplitude for each impact parameter is a function of the ratio of the inverse size of the projectile and of the *local* saturation scale.

However, the kinematical range in which formula (11) may apply is quite restricted. Let us set $\Lambda = \Lambda_\mathrm{QCD}$. We have required large impact parameters (in practice, $b > 0.2\,\mathrm{fm}$) and Q_s close to Q, which has to sit in the perturbative regime ($Q \gg \Lambda_\mathrm{QCD}$). From formula (10), one sees that the latter conditions require a large rapidity evolution, during which the saturation regime might already be reached for smaller impact parameters (i.e. $Q < Q_\mathrm{s}(b')$ for some $b' < b$). It is not possible to quantify this effect without knowing the dynamics for all impact parameters.

We shall now refer to another, maybe safer approach, which will however lead to comparable conclusions on "local" geometric scaling.

2.2 The impact parameter profile as an initial condition

In [25], the argument that the quantum evolution was quasi-local in impact parameter was developed on the basis of an analysis of the non-linear evolution equations. As a result, the dipole–proton scattering amplitude at fixed impact parameter can be written in a factorized form, because the latter feature means that the impact parameter dependence remains unchanged throughout the rapidity evolution. The non-perturbative profile of the proton is introduced as an initial condition. The validity of such a factorization has been confirmed very recently in the context of γ^*–γ^* reactions [34]. The amplitude then reads

$$\mathcal{A}_\mathrm{d}(y, Q, b) = S(b) \cdot \mathcal{T}_\mathrm{d}(y, Q) \ , \qquad (12)$$

where $\mathcal{T}_\mathrm{d}(y, Q)$ is the forward amplitude (3). Above the saturation scale, $\mathcal{T}_\mathrm{d}(y, Q)$ exhibits geometric scaling as seen on (7); thus the amplitude $\mathcal{A}_\mathrm{d}$ also scales. The profile function

$$S(b) = \frac{2}{\pi} m_\pi^2 \cdot \mathrm{e}^{-2m_\pi b} \qquad (13)$$

was postulated (we chose the normalization such that $\int \mathrm{d}^2 b\, S(b) = 1$). It involves the long-distance scale $1/m_\pi$, which is put by hand and interpreted as an initial condition.

This leads once again to a scaling of the form (11), with a local saturation scale given by

$$Q_\mathrm{s}^2(y, b) = \mathrm{e}^{-2m_\pi b/\lambda} \cdot Q_\mathrm{s}^2(y) = \mathrm{e}^{-2m_\pi b/\lambda} \cdot \Lambda_\mathrm{QCD}^2 \mathrm{e}^{\lambda y} \ . \qquad (14)$$

We see that this result is qualitatively close to (10), except for the b-dependence which is exponential rather than power-like. This stems from the fact that non-perturbative

physics with short range pion fields were introduced here, whereas previously only long-range Coulomb-like fields were considered.

At this point, it may be useful to evaluate the saturation scale at HERA from these formulae. For values of the rapidity y of the order of those measured at HERA in the small-x region ($x \sim x_0 \sim 3 \cdot 10^{-4}$), one sees from formula (14) that $Q_\mathrm{s}(b=0) \sim 1\,\mathrm{GeV}$. Q_s reaches the value of Λ_QCD at the impact parameter $b \sim 0.6\,\mathrm{fm}$. This means that for a probe of size $1/Q < 1\,\mathrm{GeV}^{-1}$, the proton looks grey everywhere and extends up to a radius of about 0.6 fm.

3 A way to check scaling at HERA

As geometric scaling at fixed impact parameter seems to be a definite prediction of saturation models, it is worth testing it against the data. A former analysis [24] has already shown the relevance of impact parameter dependent analysis in the discussion of saturation. There, the S-matrix element for dipole–proton scattering at fixed impact parameter was extracted from diffractive electroproduction of vector mesons at HERA. This quantity can be interpreted as a transparency coefficient, and thus quantifies the "blackness" of the proton as seen by the projectile. Such a kind of analysis is always model dependent, since to get the correct normalization of the S-matrix element, one has to rely on an ad hoc model for the final-state vector meson. Although it was shown in [24] that requiring that the initial state be a *longitudinal* photon limits the model dependence, an estimated uncertainty of 20% was still recognized. However, dependence of the cross section on a scaling variable can be tested in a model-independent way.

The scattering amplitude at fixed impact parameter can be extracted from differential cross sections for high energy quasi-elastic processes by a Fourier transform with respect to the momentum transfer. By quasi-elastic we mean that the initial and final states have the same number of particles. In practice, the process we are thinking of will be diffractive electro-production of vector mesons.

Let us consider such a quasi-elastic process. Its amplitude $\mathcal{A}$ is related to the differential cross section through the formula

$$\frac{\mathrm{d}\sigma}{\mathrm{d}t} = \frac{1}{16\pi}|\mathcal{A}(t)|^2 \,, \tag{15}$$

where t is the usual Mandelstam variable and all other dependences are implied. At high energies, it is well-known that the scattering amplitude $\mathcal{A}$ is essentially real. Formula (15) shows that $\mathcal{A}(t)$ is proportional to the square root of the differential cross section $\mathrm{d}\sigma/\mathrm{d}t$. A further Fourier transform with respect to the two-dimensional momentum transfer then gives the scattering amplitude for a fixed impact parameter

$$\mathcal{A}(b) = \sqrt{\pi}\int_0^{+\infty} d(-t)\, J_0(b\sqrt{|t|})\sqrt{\frac{\mathrm{d}\sigma}{\mathrm{d}t}} \,, \tag{16}$$

where J_0 is a Bessel function. For formula (16) to be valid, it is important that the quasi-elastic final state be well identified as a *single* particle or resonance. A more complex final state like $\gamma^* p \to \pi^+\pi^- p$ (which is what is actually observed in the experiments) can proceed through several different channels (with intermediate states ρ, ω, $f_0, ...$). Its study would require the careful treatment of phases and interference effects; see for example [35, 36]. We shall assume that we have a single-channel process, and we use formula (16) to extract the b-dependent amplitude from the available data.

We shall now be more specific, specializing to the case of electro-production of vector mesons $\gamma^* p \to V p$, where V will in practice be a ρ meson. The picture is the following. At high energy, the photon splits into a dipole of fixed size r which scatters off the proton before recombining into a meson. Due to its high relative velocity, the dipole does not change size during the scattering. Accordingly, the scattering amplitude $\mathcal{A}$ is the convolution of the photon wave function ψ_{γ^*}, the meson wave-function ψ_V and the dipole amplitude $\mathcal{A}_\mathrm{d}$ in the same way as in (8)

$$\mathcal{A}(y,Q,b) = \int \mathrm{d}^2 r\, \psi^\dagger_{\gamma^*}(r,Q) \otimes \psi_V(r) \cdot \mathcal{A}_\mathrm{d}(y, 1/r, b) \,, \tag{17}$$

the forward amplitude $2\mathcal{T}_\mathrm{d}$ appearing in (8) being replaced by the impact parameter dependent one $\mathcal{A}_\mathrm{d}$. Due to the fact that the product of the wave functions $\psi^\dagger_{\gamma^*} \otimes \psi_V$ is peaked around a typical dipole size depending only on the external transverse momentum scales, the scaling of the dipole amplitude $\mathcal{A}_\mathrm{d}$ (see (11)) is transmitted to the photon–proton amplitude $\mathcal{A}$. As it is well known from both empirical tests [37, 38] and experimental [39] studies, the relevant distance scale at the photon–meson vertex is a combination of the photon virtuality Q and of the meson mass M, namely $1/\sqrt{Q^2+M^2}$ instead of $1/Q$ as in the case of inclusive scattering. We then obtain from (10), (14) and (11) that the amplitude $\mathcal{A}$ in (17) should be a function of the scaling variable $\tau = (Q^2+M^2)(x/x_0)^\lambda$ only, once the impact parameter b is fixed.

To check this statement, we apply the transformation (16) to the HERA published data on electro-production of ρ^0 vector mesons. In the presently published experimental analysis [40, 41], the total cross section as well as the logarithmic t-slope B are quoted. The data can then be represented by the parameterization

$$\frac{\mathrm{d}\sigma}{\mathrm{d}t}(Q,W) = B(Q,W)\cdot\sigma(Q,W)\cdot \mathrm{e}^{-B(Q,W)|t|} \,, \tag{18}$$

up to $|t|$ of the order of $|t_\mathrm{max}| = 1\,\mathrm{GeV}^2$, which corresponds to the range in which data have been collected. The scattering amplitude at each impact parameter reads

$$\begin{aligned}\mathcal{A}(y,Q,b) &= \sqrt{\pi}\left(\int_0^{|t_\mathrm{max}|} d(-t)\, J_0(b\sqrt{|t|})\sqrt{B\sigma}\cdot \mathrm{e}^{-B|t|/2}\right.\\ &\left. \quad + \int_{|t_\mathrm{max}|}^{+\infty} d(-t)\, J_0(b\sqrt{|t|})\sqrt{\frac{\mathrm{d}\sigma}{\mathrm{d}t}}\right)\end{aligned} \tag{19}$$

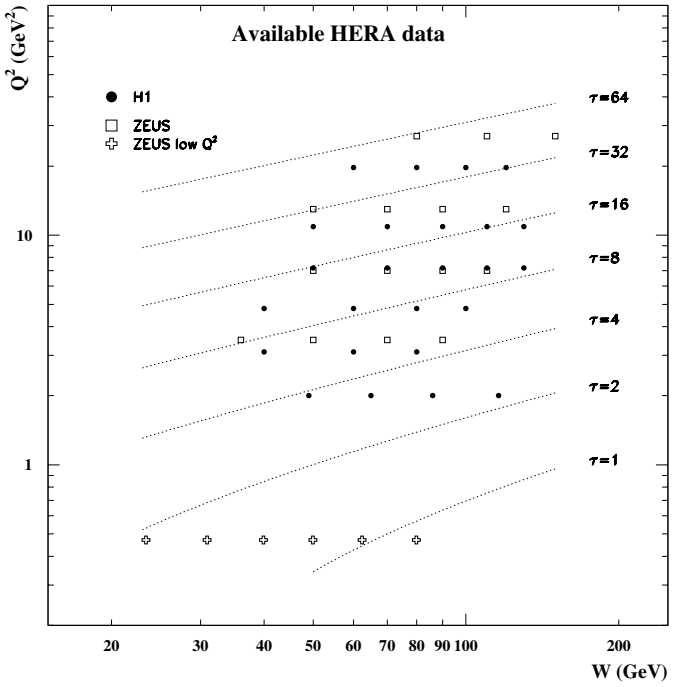

Fig. 1. Kinematics of the data on the total cross section for diffractive electro-production of ρ^0 mesons at HERA [40, 41]. The points represent the location of the data in the kinematical plane (Q^2, W). Curves of equal scaling ratio $\tau = (Q^2 + M^2)(x/x_0)^\lambda$ are shown

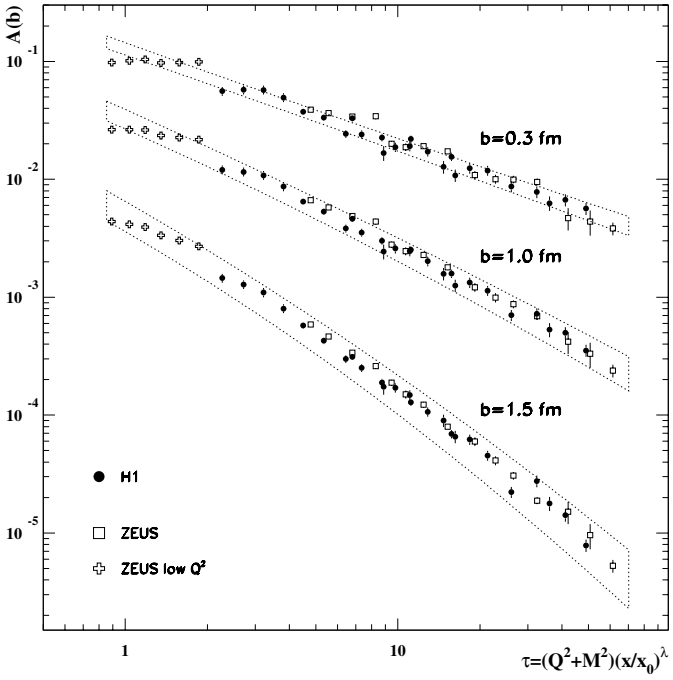

Fig. 2. Amplitude for three different impact parameters as a function of the scaling variable. The dotted contours indicate a rough estimate of the total uncertainty due to experimental error on both the total cross section σ and the slope B as explained in the text; see formula (22). The data points are derived from H1 [41] and ZEUS [40] analysis of diffractive production of ρ^0 mesons. The error bars shown take into account the uncertainty on the measurement of the total cross section only

$$\simeq \sqrt{\pi}\left(\int_0^{+\infty} d(-t)\, J_0(b\sqrt{|t|})\sqrt{B\sigma}\cdot \mathrm{e}^{-B|t|/2}\right)$$

$$= 2\sqrt{\frac{\pi\sigma(Q,W)}{B(Q,W)}}\mathrm{e}^{-b^2/2B(Q,W)}\ . \qquad (20)$$

We take the total cross section from [40, 41]. The kinematical range of these measurements is shown on Fig. 1. The experimental points range from $Q^2 = 0.47$ to $27\,\mathrm{GeV}^2$ and $W = 23.4$ to $150\,\mathrm{GeV}$. Due to the lack of data for the slope B for all values of Q^2 and W, we shall assume

$$B(Q,W) = 0.6\cdot\left(\frac{14}{(Q^2+M^2)^{0.26}}+1\right) + 4\alpha'\log(W/75)\ , \qquad (21)$$

all quantities appearing in the previous formula being expressed in powers of $1\,\mathrm{GeV}$. The parameterization (21) at $W = 75\,\mathrm{GeV}$ is taken from [42]. A logarithmic energy dependence has been added according to the Donnachie–Landshoff parameterization for the pomeron [43]. We set the Regge slope α' to the value 0.25 which is measured in hadron–hadron cross sections. The relevance of this choice and its implications will be discussed in the next section.

The results of our analysis are displayed on Fig. 2 for the three different impact parameters, $b = 0.3, 1.0$ and $1.5\,\mathrm{fm}$. Needless to say, our plot is only illustrative for the method and, being theoreticians, we cannot provide a quantitative analysis. The error bars shown take into account only the error on the total cross section ($\Delta\mathcal{A}/\mathcal{A} = (\Delta\sigma/\sigma)/2$) and the contour gives a rough idea of the total uncertainty, evaluated as if they were uncorrelated and small by the formula

$$\frac{\Delta\mathcal{A}}{\mathcal{A}} = \frac{1}{2}\frac{\Delta\sigma}{\sigma} + \frac{1}{2}\frac{\Delta B}{B}\left(1+\frac{b^2}{B}\right)\ . \qquad (22)$$

We assumed an error on the slope B of 5% which seems realistic regarding the quality of recently measured data (see the J/Ψ analysis of [44]). We see from (22) that the uncertainty on B affects mostly the large impact parameter region. For small b, an additional error would come from the fact that the data does not extend to arbitrarily large $|t|$, hence the exponential form (20) is not constrained for small b. This is the reason why we performed our analysis only down to impact parameters as large as $0.3\,\mathrm{fm}$ (see [24] for a more complete discussion).

The results on Fig. 2 are consistent with "local" geometric scaling within uncertainties, for each of the displayed impact parameters. Although the kinematical range of the data is not very large, scaling is a non-trivial feature since data points of different Q and W overlap, as seen on Fig. 1. From the technical point of view, the fact that the data should scale for various values of b is not explicit on formula (20). But one should not try to deduce too much from the analytical form of the latter, since it is only meant to be a representation of the present published data. Only its effective behavior matters. Genuine experi-

mental points for the amplitude $\mathcal{A}$ at different values of y, Q and b could be provided soon by experimental analyses and would replace formula (20). Finally, let us note that the data points denoted by a cross correspond to very low values of Q^2 ($0.47\,\mathrm{GeV}^2$), and are kinematically quite separated from the other data. As they are measured with a different method, we do not make a point of the fact that they do not seem to lie on the same curve as the larger Q^2 data.

4 Discussion and conclusion

In this paper, we have demonstrated that "local" geometric scaling, predicted by the saturation models for deep-inelastic scattering, is compatible with the HERA data. However, a consistent experimental analysis with a careful treatment of the uncertainties as well as an extension of the kinematical range is needed to draw a strong conclusion. In particular, an extension of the range in W would enable us to compare measurements sitting at very different Q^2 but at the same scaling variable τ. This would constitute a definite test of this local scaling.

Nevertheless, let us note the surprising fact that scaling seems to work well for large impact parameters, very far from the center of the proton, and even outside the "grey" zone ($b = 1.5\,\mathrm{fm}$), where the concept of saturation scale makes little sense. This feature depends of course a lot on the form of the measured B, and particularly on its energy dependence, which was introduced in an ad hoc way in (21). Interestingly enough, if the energy dependence were less steep for large momentum transfers $\sqrt{|t|}$, scaling would also be slightly better verified at small impact parameters. Such a feature is likely to happen since it seems that the harder the momentum scales, the weaker the energy dependence of the t-slope. This rule of thumb is best seen in large-t proton-dissociative photo-production of ρ mesons [45], although of course it is not a quasi-elastic process and our analysis would not apply. Moreover, recent preliminary experimental results indicate that α' is smaller than the Donnachie–Landshoff value, and decreases with the scale $Q^2 + M^2$. If scaling were confirmed also for large impact parameters, it might be an indication of some more general symmetry of high energy dynamics.

One would in principle be able to plot all data for different b as a function of a unique scaling variable $Q^2/Q_s^2(y,b)$; see formula (11). However, we checked that the parameterizations for the saturation scale proposed so far in (5) and (10) do not lead to a superposition of all points on a single curve. This means that the available approaches to the computation of the impact parameter dependence of the saturation scale are not good enough yet.

The theoretical status of the impact parameter dependence of the saturation scale is still unclear, mainly due to technical difficulties in solving the full saturation equations. Better insights into these issues would help a lot the understanding of high energy scattering within QCD. Important issues like unitarity problems require a good understanding of the evolution in impact parameter [16, 33] (see [46] for a model which predicts such an evolution). On the experimental side, diffractive vector meson production in DIS is being investigated intensively at HERA [47], and more data will be available soon. We believe that it would be worth to plot the forthcoming data in the way we propose in this paper.

Acknowledgements. This work is funded by the European Commission IHP program under contract HPRN-CT-2000-00130. We thank H.-J. Pirner for a critical reading of the manuscript and useful suggestions. We are also grateful to A. Freund, E. Iancu and B. Pire whose remarks helped us to improve the manuscript.

References

1. A.M. Staśto, K. Golec-Biernat, J. Kwiecinski, Phys. Rev. Lett. **86**, 596 (2001), hep-ph/0007192
2. A. Freund, K. Rummukainen, H. Weigert, A. Schafer, hep-ph/0210139
3. A.J. Buras, J. Dias de Deus, Nucl. Phys. B **71**, 481 (1974)
4. U. Amaldi, K.R. Schubert, Nucl. Phys. B **166**, 301 (1980)
5. I. Balitsky, Nucl. Phys. B **463**, 99 (1996), hep-ph/9509348
6. Y.V. Kovchegov, Phys. Rev. D **60**, 034008 (1999), hep-ph/9901281
7. L.D. McLerran, R. Venugopalan, Phys. Rev. D **49**, 2233 (1994), hep-ph/9309289
8. L.D. McLerran, R. Venugopalan, Phys. Rev. D **49**, 3352 (1994), hep-ph/9311205
9. L.D. McLerran, R. Venugopalan, Phys. Rev. D **50**, 2225 (1994), hep-ph/9402335
10. E. Iancu, L.D. McLerran, Phys. Lett. B **510**, 145 (2001), hep-ph/0103032
11. E. Iancu, A. Leonidov, L.D. McLerran, Nucl. Phys. A **692**, 583 (2001), hep-ph/0011241
12. E. Ferreiro, E. Iancu, A. Leonidov, L. McLerran, Nucl. Phys. A **703**, 489 (2002), hep-ph/0109115
13. M. Lublinsky, Eur. Phys. J. C **21**, 513 (2001), hep-ph/0106112
14. K. Golec-Biernat, L. Motyka, A.M. Staśto, Phys. Rev. D **65**, 074037 (2002), hep-ph/0110325
15. J. Kwiecinski, A.M. Stasto, Phys. Rev. D **66**, 014013 (2002), hep-ph/0203030
16. E. Iancu, K. Itakura, L. McLerran, Nucl. Phys. A **708**, 327 (2002), hep-ph/0203137
17. A.H. Mueller, D.N. Triantafyllopoulos, Nucl. Phys. B **640**, 331 (2002), hep-ph/0205167
18. D.N. Triantafyllopoulos, Nucl. Phys. B **648**, 293 (2003), hep-ph/0209121
19. E.A. Kuraev, L.N. Lipatov, V.S. Fadin, Sov. Phys. JETP **45**, 199 (1977)
20. I.I. Balitsky, L.N. Lipatov, Sov. J. Nucl. Phys. **28**, 822 (1978)
21. S. Munier, Phys. Rev. D **66**, 114012 (2002), hep-ph/0205319
22. M. Kuroda, D. Schildknecht, Phys. Rev. D **66**, 094005 (2002), hep-ph/0206262
23. H.J. Pirner, F. Yuan, Nucl. Phys. Proc. Suppl. **108**, 313 (2002)
24. S. Munier, A.M. Staśto, A.H. Mueller, Nucl. Phys. B **603**, 427 (2001), hep-ph/0102291

25. E. Ferreiro, E. Iancu, K. Itakura, L. McLerran, Nucl. Phys. A **710**, 373 (2002), hep-ph/0206241
26. A. Freund, (2002), hep-ph/0212017
27. H. Navelet, S. Wallon, Nucl. Phys. B **522**, 237 (1998), hep-ph/9705296
28. S. Munier, R. Peschanski, C. Royon, Nucl. Phys. B **534**, 297 (1998), hep-ph/9807488
29. A.H. Mueller, B. Patel, Nucl. Phys. B **425**, 471 (1994), hep-ph/9403256
30. N.N. Nikolaev, B.G. Zakharov, Z. Phys. C **49**, 607 (1991)
31. A.H. Mueller, Nucl. Phys. B **415**, 373 (1994)
32. K. Golec-Biernat, M. Wusthoff, Phys. Rev. D **60**, 114023 (1999), hep-ph/9903358
33. A. Kovner, U.A. Wiedemann, Phys. Rev. D **66**, 051502 (2002), hep-ph/0112140
34. S. Bondarenko, M. Kozlov, E. Levin, (2003), hep-ph/0303118
35. P. Hagler, B. Pire, L. Szymanowski, O.V. Teryaev, Phys. Lett. B **535**, 117 (2002), Erratum **540**, 324 (2002), hep-ph/0202231
36. P. Hagler, B. Pire, L. Szymanowski, O.V. Teryaev, Eur. Phys. J. C **26**, 261 (2002), hep-ph/0207224
37. J. Nemchik, N.N. Nikolaev, B.G. Zakharov, Phys. Lett. B **341**, 228 (1994), hep-ph/9405355
38. J. Nemchik, N.N. Nikolaev, E. Predazzi, B.G. Zakharov, Z. Phys. C **75**, 71 (1997), hep-ph/9605231
39. P. Marage, hep-ph/0104196
40. ZEUS, J. Breitweg et al., Eur. Phys. J. C **6**, 603 (1999), hep-ex/9808020
41. H1, C. Adloff et al., Eur. Phys. J. C **13**, 371 (2000), hep-ex/9902019
42. A.C. Caldwell, M.S. Soares, Nucl. Phys. A **696**, 125 (2001), hep-ph/0101085
43. A. Donnachie, P.V. Landshoff, Nucl. Phys. B **244**, 322 (1984)
44. ZEUS, S. Chekanov et al., Eur. Phys. J. C **24**, 345 (2002), hep-ex/0201043
45. ZEUS, S. Chekanov et al., Eur. Phys. J. C **26**, 389 (2003), hep-ex/0205081
46. A.I. Shoshi, F.D. Steffen, H.J. Pirner, Nucl. Phys. A **709**, 131 (2002), hep-ph/0202012
47. A. Levy, hep-ex/0301022